A preparation pulse for fast steady state approach in Actual Flip angle Imaging

A preparation pulse for fast steady state approach in Actual Flip angle Imaging

Marco Andrea Zampini[a,b], Jan Sijbers[c,d], Marleen Verhoye[b,d], and Ruslan Garipov[a]

[a]MR Solutions Ltd., Ashbourne House, Old Portsmouth Rd, Guildford, Surrey, GU3 1LR, United Kingdom

[b]Bio-Imaging Lab, Department of Biomedical Sciences, University of Antwerp, Belgium

[c]imec-Vision Lab, Department of Physics, University of Antwerp, Belgium

[d]μNEURO Research Centre of Excellence, University of Antwerp, Belgium

Running title: *AFI preparation pulse*

Corresponding author:

Marco Andrea Zampini - marco.zampini@mrsolutions.com - 6 Jay Ln Acton, MA 01720 (USA)

Abstract

Background: Actual Flip angle Imaging is a sequence used for B_1 mapping, also embedded in the Variable flip angle with Actual Flip angle Imaging for simultaneous estimation of T_1, B_1 and equilibrium magnetization.

Purpose: To investigate the design of a preparation module for AFI to allow a fast approach to steady state without requiring the use of dummy acquisitions.

Methods: The features of a preparation module with a B_1 insensitive adiabatic pulse, spoiler gradients, and a recovery time T_{rec} were studied with simulations and validated via experiments and acquired with different k-space traveling strategies. The robustness of the flip angle of the preparation pulse on the acquired signal is studied.

Results: When a 90° adiabatic pulse is used, the forthcoming T_{rec} can be expressed as a function of repetition times and AFI flip angle only as $TR_1(n + \cos\alpha)/(1 - \cos^2\alpha)$, where n represents the ratio between the two repetition times of AFI. The robustness of the method is demonstrated by showing that using the values further away from 90° still allows for a faster approach to steady state than the use of dummy pulses.

Conclusions: The preparation module is particularly advantageous for low flip angles, as well as for AFI sequences that sample the center of the k-space early in the sequence, such as centric ordering acquisitions, and for ultrafast EPI-based AFI methods, thus allowing to reduce scanner overhead time.

Keywords — Actual Flip angle Imaging, preparation pulse, T_1 mapping, B_1 field, EPG simulations

1 Introduction

The longitudinal relaxation time T_1 has been in the spotlight for being a promising and versatile biomarker for dementia, multiple sclerosis[1], epilepsy[2], and for tumor identification and characterization[3,4,5,6]. On top of biological and patho-physiological variability, T_1 mapping techniques report a wide range of T_1 values in tissues, raising the issue of protocols reproducibility and standardization[7,8,9,10,11,12,13]. As accuracy is a requirement for using quantitative MRI in clinical applications, one needs to investigate and isolate confounding factors of signal variability: for example, T_1 mapping can not overlook knowledge of the excitation field B_1, with B_1 inhomogeneity affecting T_1 accuracy especially at high magnetic field[14].

Actual Flip angle Imaging (AFI) is a gradient echo based sequence employed for fast B_1 mapping[15] with a low Specific Absorption Rate (SAR)[16]. The excitation field is estimated by a robust and simple approximation based on the negligible ratio between the repetition times of the sequence and the T_1 ($TR \ll T_1$) of commonly scanned tissues, which warrant the method validity for a broad range of T_1 values. Although AFI has been investigated as a 3D method, 2D implementations of AFI for fast single-slice mapping have been published for B_1 mapping as well[17,18].

AFI is commonly used as a stand-alone module, but it was also embedded in the VAFI (Variable flip

angle - Actual Flip angle Imaging) method, which relies on the acquisition of an AFI and at least one SPoiled GRadient echo (SPGR) acquisition to perform the joint estimation of T_1, B_1 and equilibrium magnetization[19]. Indeed, as AFI is characterized by a low SAR and SPGR volumes are typically acquired fast and with low energy deposition, VAFI can be employed for accurate, fast, low-SAR T_1 mapping at high magnetic field. Both AFI and SPGR acquisitions require the signal to be acquired at steady state (SS), so the spoiling properties and the transient approach need to be investigated.

As for many SS sequences, samples at the beginning of an AFI sequence are usually discarded in order to acquire a signal close to SS. However, to our knowledge, the approach to SS for an AFI sequence has not been discussed and no alternatives have been published so far. As a result, the number of discarded acquisitions (or dummy pulses) is chosen arbitrarily, ranging from as little as 8 to 600 dummy pulses[15,20]. A high number of dummy pulses can impact negatively the length of the acquisition overhead time, while an insufficient number or discarded pulses can result in artifacts in the image due to clipping or to an incorrect weighting of k-space lines. These artifacts can be detrimental and impair parameter mapping especially in centric ordering acquisitions, EPI-based acquisitions, and in highly accelerated sequences. A preparation pulse has been proposed for fast SS approach for SPGR acquisitions[21] relying on a single saturation pulse, but possible flip angle deviations due to B_1 field inhomogeneity could invalidate the benefit of using a preparation pulse, keeping the approach to SS long. A more efficient preparation pulse for SPGR and AFI acquisitions would be useful for a new, fast approach to SS and to avoid possible artifacts arising from signal transient-state.

Here, we propose a new preparation pulse for the AFI sequence, we study its characteristics and describe the features for B_1 inhomogeneities robustness. We validate the use of the preparation pulse via AFI signal comparisons and B_1 map estimation in phantoms, and ex vivo on a mouse brain.

2 Methods

2.1 Actual Flip angle Imaging

Actual Flip angle Imaging (AFI) was originally proposed by Yarnykh as a method for a fast and low-SAR B_1 computation and is also employed in the inhomogeneity correction for accurate T_1 mapping[20,22,23,24,25,26,27].

AFI steady-state signals can be derived by solving the Bloch equations for a sequence with asymmetric repetition times, which provides[15]

$$S_{AFI1,2} = M_0 \sin\alpha \cdot \frac{1 - E_{2,1} + (1 - E_{1,2})E_{2,1}\cos\alpha}{1 - E_1 E_2 \cos^2\alpha} \exp(-\mathrm{TE}/\mathrm{T}_2^*) = M_0 \sin\alpha \cdot \exp(-\mathrm{TE}/\mathrm{T}_2^*) A_{1,2} \quad (1)$$

where M_0 represents the net magnetization signal, α represents the flip angle, $E_{1,2} = \exp(-\mathrm{TR}_{1,2}/\mathrm{T}_1)$, n represent the ratio between TR_2 and TR_1, $A_{1,2}$ represents a dimensionless measure of the SS longitudinal magnetization, and the subscripts 1 and 2 represent the respective repetition times.

The computation of B_1 maps in AFI assumes that $\mathrm{TR}_{1,2} << \mathrm{T}_1$ applies for the scanned tissues, for

which $E_{1,2}$ can be approximated by 1, so that the flip angle can be computed as

$$\alpha \approx \arccos \frac{S_{AFI2}/S_{AFI1} \cdot n - 1}{n - S_{AFI2}/S_{AFI1}} \quad . \tag{2}$$

Although originally used as a 3D technique, AFI has been used for 2D data acquisition and can be adapted to acquire multislice 2D data. As 2D encoding leads to systematic errors in the computation of the transmit field B_1 values, accurate mapping can be achieved by using RF pulses with adequate spatial excitation profile, and reducing the slice cross-talk, as well as by the implementation of slice profile correction strategies[28]. These help in mitigating measurement errors and in producing reliable B_1 maps for arbitrarily chosen slice selective RF pulses, opening the possibility to implement the technique in an interleaved or distributed fashion[29] while improving time efficiency.

SPGR-based sequences are sampled at SS to match the model expression and to avoid artifacts caused by signal approach to stabilization. Normally, an arbitrary number of RF pulses (dummies) is provided and discarded before reaching the regime condition at SS. Ideally, a preparation module would make the magnetization vector reach its SS value with just one RF pulse and a subsequent recovery time whose duration is analytically defined and independent on imaged tissue properties. While a preparation module consisting of a saturation pulse was proposed for SPGR sequences[21], this remains rarely employed in practice, and, to our knowledge, no preparation module has been proposed for AFI yet. Advantages of the application of a magnetization preparation pulse include lower energy deposition (as SAR $\propto B_1^2$) and an almost immediate SS approach, which can help with fast and ultra-fast SPGR-based acquisitions.

2.2 Preparation pulse

In AFI sequences, the number of dummy pulses for SS approach is relatively low. However, a preparation pulse would make it faster, irrespective of the tissue characteristics, which can be of special interest for multi-slab and multi-slice acquisitions, when the centric or radial k-space acquisition scheme is utilized, and for AFI sequences acquired with an EPI readout. Indeed, centric acquisitions first sample the central region of the k-space to then move outwards (center-out), while EPI acquisitions travel through the central region of the k-space at every shot, which could result in signal artifacts and distortions if the magnetization has not reached SS yet. Preparation in center-out acquisitions is normally achieved by the application of dummy pulses. Nevertheless, highly accelerated and time-critical fast and ultra-fast acquisitions would benefit from the application of a preparation pulse.

Signal simulations are needed for the analysis and determination of the preparation pulse features. These also need to include RF phase effects for the study of the time evolution of the magnetization vector: the analysis of echoes and their generation can be studied via Extended Phase Graph (EPG) model[30,31,32]. This powerful model generates the signal from an isochromat ensemble and uses matrix operations to describe the effects of the sequence components and sequence-related effects such as gradients, RF pulses, motion, relaxation and diffusion on configuration states representing the magnetization dephasing coordinates.

The signal for the j-th AFI pulse can be described analytically by the solution of Bloch equations, by recursively exploiting the expression for the SS approach of SPGR sequences, assuming the signal is

perfectly spoiled. Analytically, for $j \geq 1$ each pulse has an offset from SS value of $(\cos\alpha\, E_{1,2})^{j-1}(1-A)$ so that when the magnetization has experienced a total of $2j-2+i$ pulses and $i = 1, 2$ for $\mathrm{AFI}_{1,2}$, respectively, the signal in this ideally spoiled scenario is

$$S_{j,i} = M_0 \sin\alpha[A_i + (\cos\alpha\, E_1)^j(\cos\alpha\, E_2)^{j-1}(1-A_i)]\exp(-\mathrm{TE}/\mathrm{T}_2^*) \quad . \tag{3}$$

SS longitudinal magnetization of the AFI sequence ($M_0 A_1 = S_{AFI1,2}/(\sin\alpha\exp(-\mathrm{TE}/\mathrm{T}_2^*))$) can be matched to the magnetization value after an arbitrary β pulse and a free relaxation period T_{rec}:

$$M_z(T_{rec}) = M_0[1-(1-\cos\beta)\exp(-T_{rec}/\mathrm{T}_1)] \tag{4}$$

which cancels out the magnetization term M_0 from the equation and gives the recovery times required to reach the SS of AFI_1 signal, which should be reached after the preparation pulse (although an analogous expression can be similarly derived for AFI_2):

$$T_{rec} = \mathrm{T}_1 \log\Big(\frac{1-\cos\beta}{1-A_1}\Big) \quad . \tag{5}$$

2.3 Simulations

To show the duration of AFI without any preparation, the effects of repetition time, n and the error threshold defined as $\epsilon = 100 * |S_{j,1} - S_{AFI1}|/S_{AFI1}$ on the signal variability as a function of the flip angle α and T_1 was studied for a $\mathrm{TR}_1/\mathrm{T}_1$ ratio from 0.005 to 0.05.

To ensure a spatially homogeneous excitation with the preparation β pulse, we employed an adiabatic pulse with a hyperbolic secant profile as a preparation pulse because of its high tolerance to B_1 field variations over the excitation volume that could be significant, especially for 3D acquisitions[29,33]. However, due to the higher pulse amplitude (and SAR) and longer duration, adiabatic RF pulses are rarely employed as imaging (α) pulses. We report T_{rec} for AFI after an application of the β pulse with an amplitude of 86 to 94° for $\alpha = 60°$ and T_1 values increasing from 0 to 5 s, computed from Equation 5. Also, we investigated the effects of T_2 on the approach to SS for a prepared and a non-prepared AFI sequence for $\mathrm{T}_1 = 1.5$ s, $\mathrm{T}_2 \in [0.01, 0.2]$ s, $\alpha = 40°$, $D = 1 \cdot 10^{-3}$ mm^2/s.

As the time employed by the preparation time T_{rec} will depend exclusively on tunable parameters, we report a plot of T_{rec} in AFI units corresponding to $\mathrm{TR}_1(n+1)$ as a function of the flip angle for $n =$ 4, 5, 6.

Simulations to check the effects of the β pulse amplitude on AFI_1 were performed via an EPG approach with analogous parameters and with $\mathrm{T}_1 = 2.52$ s, $\mathrm{T}_2 = 0.01$ s, gradient spoiling = 327 and 1415 mT·ms/m for TR_1 and TR_2, respectively, and diffusion coefficient $D = 1 \cdot 10^{-3}$ mm^2/s for flip angles of 30° and 60°. β was set as an equispaced array of flip angles ranging from 84 to 96°. Values around 90° are reported to simulate the effect of possible imperfections in the flip angle of the preparation RF pulse on the recovery time T_{rec}, while the value $n = 5$ was chosen within the range of n values from the original publication with sufficient sensitivity to flip angle variations. Simulation TR values were chosen under 100 ms, also in agreement to the original AFI publication, to better exploit the speed of SPGR-based sequences. We also report the behavior of AFI_1 signal following a non-adiabatic preparation

pulse, which was simulated by scaling the saturation pulse by the empirically computed scaling factor or normalized B_1 value $\kappa = B_1/\alpha$, and the simulated behavior for the respective B_1 relative percent difference values, where B_1 was computed via Equation 2 and the difference values were computed as $100 * |B_1 - \alpha_{nominal}|/\alpha_{nominal}$.

A slice profile correction was implemented for the computation of B_1 values following the approach of Malik[28]. Numerical integration of Bloch simulations solved for a 3 lobes sinc pulse, for the relevant gradient waveforms parameters and for an array of B_1 values was used to obtain the flip angle distribution and the signal received with 2D spatial encoding, estimated by integration over the slice thickness. T_1 and T_2 values were matched to those computed from experimental values when available, else $T_1 = 1000$ ms was used and the effects of transverse relaxation were neglected according to the original slice profile correction method. The simulated values for the ratio S_{AFI2}/S_{AFI1} were used to create a lookup table and B_1 values were retrospectively linearly interpolated from it.

The main sequence parameters for AFI acquisitions and physiological values used for the simulations are also summarized in Table **??**.

2.4 Experiments

Experiments were performed on 4.7 T and 7 T MR Solutions (MR Solutions Ltd, Guildford, United Kingdom) preclinical scanners with 38 mm ID quadrature coils. The AFI sequence was developed starting from a SPGR sequence by adding a hyperbolic secant adiabatic pulse for B_1 insensitivity (BW = 3 kHz) followed by a spoiler gradient in the read and slice direction to crush the remaining transverse signal in a preparation module occurring only once at the beginning of the acquisition.

A homogeneous gelatin phantom at 16°C was used to validate the use of the proposed preparation module on a 4.7 T system, testing the approach to SS for the AFI sequence with and without the use of the described preparation pulse. T_1 ground truth values were computed through a 3-parameter fit of 22 points Inversion Recovery Spin Echo data to allow for deviations of the inversion angle[34,35] (TR = 10000 ms, TE = 16 ms, slice thickness = 2 mm, FOV = (20x20) mm^2, matrix size = [64x64], 22 TI $\in$ [5; 3500] ms). AFI acquisitions on the gelatin phantom were run with $TR_1 = 20$ ms, TE = 3 ms, $n = 5$, $\alpha_{\mathrm{AFI}} = 60°$. A 2D AFI was performed on a gelatin phantom on a 3 T system in order to evaluate the effect of the preparation pulse on RF cycling (slice thickness = 2 mm, FOV = (20x20) mm^2, matrix size = [64x64]) and to investigate of the impact of β amplitude and pulse features on the SS. We compared the effects of using an adiabatic (hyperbolic secant pulse, $\beta \in [84; 96]°$), non-adiabatic (3 lobe sinc pulse) preparation pulses both with BW = 3 kHz and no preparation on the approach to SS (slice thickness = 2 mm, FOV = (20x20) mm^2, NEX = 20).

A phosphate-buffered saline phantom with 5 different Gadolinium contrast concentrations in tubes was used to acquire B_1 values and compare the central slice of a 3D dataset used as a reference (TR_1 = 200 ms, $n = 4$, TE = 3 ms, slab thickness = 16 mm, FOV = (40x40x16) mm^2, matrix size = [128x128x16]) with 2D data acquired with a center-out k-space linear trajectory with no dummies, with 1 and 2 dummies, with the proposed preparation pulse, and with a conventional linear out-center k-space trajectory ($TR_1 = 200$ ms, $n = 4$, TE = 3 ms, slice thickness = 1 mm, FOV = (40x40) mm^2, matrix size

= [128x128]). T_1 ground truth values were computed through a 4-parameter fit of Look-Locker data (TR = 10 ms, TE = 50-5130 ms, slice thickness = 2 mm, FOV = (40x40) mm^2, matrix size = [138x138]), while T_2 ground truth values were computed via a mono-exponential fit of Multi-Echo Multi-Shot (MEMS) data (TR = 1400 ms, TE = 15-150 ms, slice thickness = 1 mm, FOV = (40x40) mm^2, matrix size = [128x128]). The S_{AFI2}/S_{AFI1} ratio values were then linearly interpolated from those found in the lookup table of values simulated from the respective T_1 values, and B_1 values were then subsequently computed via Equation 2.

A 2D ex vivo validation of the preparation pulse was performed on a mouse brain (TR_1 = 100 ms, $n = 5$, TE = 3 ms - 3D: slab thickness = 16 mm, FOV = (40x40x16) mm^2, matrix size = [128x128x16]; 2D: slice thickness = 1 mm, FOV = (40x40) mm^2, matrix size = [128x128]), acquiring images with the same protocol used for the phosphate-buffered saline phantom.

In order to demonstrate flexibility of the proposed preparation module, we also compared the effects of the preparation pulse on the B_1 map reconstructed from the first acquired image from a 2-shot 2D AFI sequence acquired with EPI readout (with the recently published sequence EPIFANI[36]) and no dummies, 1 and 2 dummy pulses on the same ex vivo sample of mouse brain immersed in agar. In this case, for both AFI and EPIFANI, no assumptions on T_1 were made and T_2 relaxation effects were ignored for the generation of the lookup table used for the slice profile correction, to test the generalization power of the correction method according to the original slice correction method publication[28].

We report Bland-Altman plots of the distribution of the κ map, namely the B_1 map normalized by the nominal flip angle $\kappa = B_1/\alpha$, for specific Regions of Interest in both the phosphate-buffered saline phantom and the ex vivo mouse brain. In the former, we provide an example of the κ line profile for all the acquisitions performed.

The experiments were run with the application of a spoiling gradient along the readout and slice direction. The RF pulse phase characteristic ϕ_0 was selected as 25° (see Section S3) and gradient moments were chosen as 327/1415 mT·ms/m (for TR_1 and TR_2, respectively), in order to reach high signal spoiling[37].

The main sequence parameters for AFI acquisitions and physiological values used for the experiments are also summarized in Table **??**.

3 Results

3.1 Preparation pulse features

The number of discarded acquisitions to reach SS with a good approximation is a function of the sequence parameters. The level plot in Figure **??** shows the number of AFI pulses required for a relative error $\epsilon < 5\%$ for an AFI sequence without preparation, where the signal was simulated via Equation 3 and ϵ is defined as the absolute normalized distance from the SS signal. The selection of the flip angle greatly impacts the approach to SS, as already demonstrated for SPGR sequences (refer to Supplementary Materials **??** for the corresponding behavior in SPGR acquisitions). Increase in the repetition time and

in n, as well as a larger admissible error ϵ reduce the number of discarded acquisitions required for signal accuracy, shifting the level lines of the plot towards lower $\mathrm{TR}_1/\mathrm{T}_1$ values, which is indicated by the black arrow.

Dependency of the recovery time T_{rec} over T_1 is shown in Figure **??**, where the flip angle β of the preparation pulse determines the curve slope for the long T_1s. This T_1 dependency becomes negligible for $\beta = 90°$ in the range of T_1 commonly found in physiological tissues ($\mathrm{T}_1 > 0.5$ s). Thus, for the considered interval the following applies (refer to Supplementary Materials S2 for the formula derivation):

$$T_{rec}(\beta = \pi/2, \mathrm{T}_1 \to \infty) = \mathrm{TR}_1 \frac{n + \cos\alpha}{1 - \cos^2\alpha} \quad . \tag{6}$$

The relative change of T_{rec} for $\mathrm{T}_1 > 0.5$ s reduces to below 2.1% and asymptotically approaches zero when $\beta = 90°$ – the analysis of the partial derivative $\partial T_{rec}/\partial \mathrm{T}_1$ is reported in the Supplementary Materials S2. In case of $\beta \neq 90°$, the curve diverges and hence no unique T_{rec} can be defined for a range of T_1 values.

Figure **??** shows the duration of the recovery time following the preparation pulse T_{rec} in terms of full AFI acquisitions (or AFI units, defined as $\mathrm{TR}_1(n+1)$), so to compare the duration of the preparation module with respect to that of dummy pulses. For flip angles within the 30-80° range and for $n = 4$, 5, 6, the recovery time T_{rec} of the preparation module is shorter than 4 repetitions of the AFI sequence, with increasing sensitivity for smaller flip angles. Thus, the duration of the preparation module T_{rec} is shorter than a preparation achieved with dummies, as at least 5 dummies are required for SS approach according to the level plot for flip angles in the 30-80° range.

Using the β values around the nominal value of 90° considerably reduces signal variability in the first RF pulses, and reduces the time required to reach SS as compared to not applying the preparation pulse. An example of the dependency of the preparation pulse efficiency over a range of β values, in both simulations and experiments, is presented in Figure **??**. The lowest mean signal variability in terms of signal range is reached for $\beta = 90°$ – a saturation pulse – but applying a preparation pulse with an amplitude close to the optimal flip angle is still more effective in approaching the SS with respect to the application of dummy pulses. Simulation results (on the left column of Figure **??**) are in agreement with the experimental data (right column), which show the signal of AFI_1 after the application of the preparation pulse approaching SS values (reported as a dashed gray line) faster than without any preparation.

Figure **??** also reports the signal behavior for AFI_1 following the application of non-adiabatic and adiabatic preparation pulses. Signal intensities values are reported in arbitrary units 'a.u.' which represent fractions of the equilibrium magnetization multiplied by several factors including the transverse relaxation decay, receiver gain, and coil sensitivity profiles. The adiabatic pulse allows to sample the SS signal immediately after the preparation pulse, reproducing the attended behavior of the simulations, while a non-adiabatic pulse can show deviations in the effective flip angle due to the inhomogeneity of the B_1 field. Also, the values of the non-adiabatic preparation pulse match the experimental values for a preparation pulse provided with a flip angle of around 81°. The different length of the transient state for $\alpha = 60°$ (top row) and 30° (bottom row) is shown, with $\beta = 90°$ providing the closest signal to SS

in both cases. Row (a) shows $\alpha = 60°$, for which T_{rec} takes 146.6 ms, while a single AFI cycle takes 120 ms. The SS is reached after approximately 6-9 cycles taking 720-1080 ms in total. Row (b) shows $\alpha = 30°$, for which T_{rec} takes 469.3 ms, and SS is reached after more than 15 cycles (> 1.8 s).

B_1 relative percent difference values follow a similar trend with respect to the absolute AFI signals: Figure **??** report simulations (left column) for $\alpha = 60°$ (top) and $\alpha = 30°$ (bottom), and data simulated without any preparation module (black line) show the highest difference with respect to the nominal B_1, while the non-adiabatic 90° pulse (green line) allows a faster approach to the SS value. The adiabatic pulse (purple line) reaches SS B_1 values almost immediately after T_{rec}. This is also confirmed by experimental data (right column), which follows the same relative trend, with the applications of dummies being the slowest approach.

EPG simulations also demonstrate how the preparation module allows a faster sampling of the SS with respect to the signal achieved without preparation. A similar behavior is followed by both AFI_1 and AFI_2 (not shown). For increasing T_2 values in particular the lack of the preparation module or dummy pulses results in a prolonged oscillation around SS (Figure **??**).

A comparison on a phantom containing a phosphate-buffered saline solution is reported in Figure **??**: the κ values (B_1 normalized by the nominal flip angle) computed from an acquisition performed with no preparation pulse and no dummies show are inaccurate with a mean systematic difference of -39.2% with respect to the reference values from a 3D AFI acquisition. As shown in the dotted values along the line profile in Figure **??** and the reconstructed κ maps of Figure **??**, some values can not be interpolated from the lookup table used for slice profile correction. This results in unreliable and unusable maps for the data acquired with no preparation and no dummies. All other acquisitions show fewer values that can not be matched with the lookup table and can be attributed to noise fluctuations. By selecting a Region of Interest at the center of the phantom (Figure **??**), the highest accuracy with respect to the reference B_1 values from a 3D AFI is reached with the preparation pulse (mean difference -6.0%), values in the case of an out-center acquisition scheme, center-out with one dummy, and two dummies are -9.2%, -14.2%, and -6.6%, respectively. Similarly, when compared to the average of the κ values in the Gadolinium solutions, the systematic difference is -5.6% for a out-center acquisition, -32.9% with no preparation, -10.9% and -7.6% with one and two dummies, and -6.4% with the preparation module, respectively (Figure **??**). The preparation with dummies took 1000 ms and 2000 ms for a single and two dummies, while the proposed preparation module required 1200 ms.

The analysis of images acquired on an ex vivo mouse brain phantom in Figure **??** further confirms what was found for the phosphate-buffered saline phantom. Presenting the images with the same intensity scale shows that the images acquired before the stabilization of the signal around SS (images with no preparation, one and two dummies) have a higher signal intensity, which results in systematic errors in the computed B_1 and, thus, κ values. The Bland-Altman plot referring to the brain report mean κ difference values of 2.0% (out-center), -21.4% (no preparation), -6.2% (one dummy), -3.1% (two dummies) and 2.2% (preparation module) with respect to the conventional 3D version of AFI. Analogously, mean difference value in the agar were 10.3% (out-center), -19.4% (no preparation), -5.7% (one dummy), -1.5% (two dummies), and 4.1% (preparation module). The preparation with dummies in this AFI example

took 600 ms for each dummy, while the proposed preparation module required 733 ms.

With EPIFANI, an AFI sequence utilizing an EPI readout[36], the first set of AFI images acquired without preparation or discarded acquisitions shows an artifact in the reconstructed image and relative κ map (Figure **??**). The SS κ reports a difference of 0.5%, while images acquired without preparation, with a dummy, two dummies and the preparation module show a bias of -5.8%, 0.5%, -0.9%, and -0.1%, respectively. This bias is higher when considering the agar: -9.6% (SS), -8.3% (no preparation), -8.1% (one dummy), -8.7% (two dummies), and -10.3% (preparation module). The preparation with dummies in this EPIFANI example took 3000 ms for each dummy, while the proposed preparation module required 3666 ms.

4 Discussion

We demonstrated the rationale for the use and efficiency of a preparation module for fast SS approach in AFI sequence. Experimental results validate theoretical findings, which confirm the robustness of the preparation pulse.

We presented the characteristics of a preparation pulse and the analytical expression for the subsequent recovery time to reach SS without using discarded acquisitions. The preparation module is composed of an adiabatic 90° RF pulse, spoiler gradients in non-encoding directions, and a recovery time T_{rec}. We found that for short repetition times, tissues with $T_1 > 0.5$ s require the same amount of time T_{rec} to allow longitudinal magnetization to recover to steady-state levels and that T_{rec} depends exclusively on the tunable sequence parameters (TR_1, n and flip angle). The fundamental independence of T_{rec} on T_1 has been demonstrated analytically for a saturation pulse: indeed, by choosing the T_{rec} value that is reached asymptotically for increasing T_1s, this preparation pulse can be applied to achieve steady-state in the majority of biological tissues of interest in neuroimaging at high magnetic field minimizing the dependency over the actual relaxation time of the imaged specimen. Due to the sensitivity of T_{rec} and, consequently, of $M_z(T_{rec})$, to the flip angle, the preparation pulse should deliver a flip angle as close as possible to 90°, which is easily ensured by the RF pulse calibration, as this represents a widespread amplitude reference[38]. Nevertheless, the use of an adiabatic pulse is robust to variations of the β amplitude and better allows SS to be reached faster than with the application of dummy pulses or in the case of B_1 inhomogeneities, which are a main drawback when scanning at high magnetic field. Further studies could focus on the impact on the signal of multiple consecutive saturation pulses in a WET-like approach[39], which could provide further $B_0/B_1/T_1$ robustness in the elimination of the transverse magnetization.

The application of such preparation module both speeds up the approach to SS and allows an accurate computation of B_1 values right after its application, without the need to provide further dummy pulses, as demonstrated in both simulations and experimental results. Also, it can be particularly advantageous for tissues with short T_2 and for acquisition methods that sample the center of the k-space early in the sequence. We have shown that imaging CSF mimicking tissues with long T_2 such as phosphate-buffer saline solution and agar still benefits from the application of the preparation module as the signal from

a prepared sequence has a faster approach to SS conditions, leading to lower signal offsets within the first RF pulse excitations.

The time benefit of the application of a preparation pulse could be majorly appreciated when employing parallel imaging with acceleration factor $R > 1$, for 2D multislice imaging, for acquisitions with a center-out k-space trajectory (spiral, radial, linear), especially at high field where long tissue T_1 values are expected (such as CSF[40], with $T_1 > 4$ s). Further applications could be found in fast breath-hold AFI acquisitions, which could be used to avoid the many dummy pulses needed to ensure operation at SS[41] and serve as both a SAR-efficient static and dynamic way to map RF transmission, thus allowing T_1 mapping correction for cardiac and abdominal imaging. Simulations show that in the range of flip angles commonly used for AFI, the preparation pulse allows reaching the SS in less than 4 full dummy acquisitions for any repetition time employed and for any tissue analyzed (around 1.25 AFI units for $\alpha = 60°$), resulting in a faster SS approach, which is otherwise would take at least 5 dummies.

Also, the recovery time T_{rec}, when expressed in times of AFI units, does not fundamentally dependent on the parameter n.

When compared to a conventional 3D AFI acquisition, we have shown that the use of the proposed preparation module for 2D AFI helps in increasing the accuracy of κ, thus B_1 values, with respect to acquisitions performed without any preparation or with dummy acquisitions with a fundamentally equivalent duration. This was shown in both a uniform phosphate-buffered saline solution with multiple Gadolinium concentrations and with an anatomical model provided by an ex vivo mouse brain.

A recently proposed[36] AFI-based T_1 mapping technique with EPI readout, EPIFANI, could also benefit from the use of a preparation pulse. We reported examples of normalized B_1 maps computed on an ex vivo mouse brain acquired with EPIFANI and found that the preparation pulse helps in preserving the accuracy of the B_1 values in the foreground (the mouse brain itself) and in the agar, although lower accuracy is reached in latter probably due to its long T_2 values.

It should be noted that a slice profile correction needs to be performed for both 2D cartesian AFI and its corresponding EPI version, taking into account the physiological parameter, specific RF pulse excitation, and the employed sequence parameters to produce reliable and accurate B_1 maps. Nevertheless, the use of a fixed value for the T_1 and neglecting the transverse relaxation – as suggested in the original slice profile correction method[28] – still provides reliable values which closely approach those computed from the reference 3D AFI acquisition.

AFI represents one of the choices for B_1 mapping, but other fast techniques have been proposed in the last decades, including methods based on adiabatic phase imaging[42], orthogonal-α[43], stimulated echo/spin echo imaging[44], saturated Turbo FLASH[45], Bloch-Siegert shift imaging[46]. AFI, nevertheless, remains one of the most commonly employed B_1 mapping reference sequences[25,20,47,48,49,26] due to its rapidity and robustness in B_1 mapping. It has been shown that 2D EPI readouts have only a small influence on the flip angle uncertainties thanks to the preceding preparation and/or long repetition times[16]. Further studies on the 2D applications of B_1 methods should focus on possible effects of out-of-bandwidth magnetization and signal pollution from distal regions to the imaged slice[50].

In center-out, radial and small matrix-size acquisitions, artifacts given by an incorrect weighting

of k-space lines appear when the signal is sampled before it reaches SS conditions and where signal oscillations affect the image contrast. Data clipping artifacts are an extreme example of this effect, which could appear in center-out acquisitions when no sequence preparation is performed. The use of the preparation pulse or dummy pulses mitigates the effects of these artifacts, thus enabling fast center-out acquisitions for both qualitative and accurate quantitative assessments. We demonstrated potential impact of the preparation pulse on parametric maps computed with an AFI approach. Although centric-view ordering schemes are typically used for reduction of motion artifacts[51] either within the context of rapidly changing (dynamic) contrast or to capture transient effects[52] rather than SS effects, the application of a preparation pulse can find an application in both ultrafast EPI-based AFI sequences and centric-view ordering sequences: the former ones could be used for dynamic B_1 mapping in order to reduce artifacts of single-shot EPI such as blurring due to the T_2^* decay and geometric distortion due to off-resonance effects[53]. Centric-view ordering sequences instead could use only the central part of the k-space of poor SNR AFI acquisitions: as B_1 profiles are usually smooth, acquiring only the central lines of the k-space – taking care of the ringing artifacts caused by k-space truncation – could reduce the total acquisition time while increasing the SNR[54]. Furthermore, the computation of B_1-corrected T_1 maps via VAFI can benefit from the use of the preparation pulse, when both 2D multislice or 3D maps are computed starting from AFI and SPGR acquisitions. As a final note, the features of the preparation module have been described for AFI. Nevertheless, they can be applied without loss of generality to any SS dual-TR sequence when used on tissues with a longitudinal relaxation time that respects the AFI assumption ($T_1 >> TR_{1,2}$)[55].

5 Conclusion

A preparation module composed of an adiabatic pulse, spoiler gradients and a recovery time was proposed for a fast steady-state approach of signal for the AFI sequence, which represents a steady-state method for B_1 mapping. The approach is robust to variations of the pulse amplitude, the analytical expression of the recovery time is T_1-independent and all tissues require approximately the same amount of time to recover to steady-state levels of longitudinal magnetization. The advantages of using a preparation module include the elimination of discarded acquisitions and artifacts that occur at the beginning of an acquisition with EPI readout or center-out k-space trajectories.

6 Acknowledgments

This research was funded by the B-Q MINDED EU H2020 project under grant agreement No.764513.

Conflict of Interest Statement

Marco Zampini and Ruslan Garipov are employees of MR Solutions Ltd.

References

[1] Vrenken H, Geurts JJ, Knol DL, et al. Whole-brain T1 mapping in multiple sclerosis: global changes of normal-appearing gray and white matter *Radiology.* 2006;240:811–820.

[2] Conlon P, Trimble MR, Rogers D, Callicott C. Magnetic resonance imaging in epilepsy: a controlled study *Epilepsy Res.* 1988;2:37–43.

[3] Eis M, Els T, Hoehn-Berlage M. High resolution quantitative relaxation and diffusion MRI of three different experimental brain tumors in rat *Magn Reson Med.* 1995;34:835–844.

[4] Herrmann K, Johansen ML, Craig SE, et al. Molecular imaging of tumors using a quantitative T1 mapping technique via magnetic resonance imaging *Diagnostics.* 2015;5:318–332.

[5] Müller A, Jurcoane A, Kebir S, et al. Quantitative T1-mapping detects cloudy-enhancing tumor compartments predicting outcome of patients with glioblastoma *Cancer Med.* 2017;6:89–99.

[6] Castets CR, Koonjoo N, Hertanu A, et al. In vivo MEMRI characterization of brain metastases using a 3D Look-Locker T1-mapping sequence *Sci. Rep.* 2016;6:1–9.

[7] Tsialios P, Thrippleton M, Glatz A, Pernet C. Evaluation of MRI sequences for quantitative T1 brain mapping in *J. Phys. Conf. Ser*;931:012038 2017.

[8] Leutritz T, Seif M, Helms G, et al. Multiparameter mapping of relaxation (R1, R2*), proton density and magnetization transfer saturation at 3 T: A multicenter dual-vendor reproducibility and repeatability study *Human brain mapping.* 2020;41:4232–4247.

[9] Lee Yoojin, Callaghan Martina F, Acosta-Cabronero Julio, Lutti Antoine, Nagy Zoltan. Establishing intra-and inter-vendor reproducibility of T1 relaxation time measurements with 3T MRI *Magnetic resonance in medicine.* 2019;81:454–465.

[10] Cooper G, Hirsch S, Scheel M, et al. Quantitative multi-parameter mapping optimized for the clinical routine *Frontiers in Neuroscience.* 2020;14:1290.

[11] Buonincontri G, Biagi L, Retico A, et al. Multi-site repeatability and reproducibility of MR fingerprinting of the healthy brain at 1.5 and 3.0 T *Neuroimage.* 2019;195:362–372.

[12] Weiskopf N, Suckling J, Williams G, et al. Quantitative multi-parameter mapping of R1, PD*, MT, and R2* at 3T: a multi-center validation *Neurosci.* 2013;7:95.

[13] Gracien RM, Maiworm M, Brüche N, et al. How stable is quantitative MRI?–Assessment of intra-and inter-scanner-model reproducibility using identical acquisition sequences and data analysis programs *Neuroimage.* 2020;207:116364.

[14] Stikov N, Boudreau M, Levesque IR, Tardif CL, Barral JK, Pike GB. On the accuracy of T1 mapping: searching for common ground *Magn Reson Med.* 2015;73:514–522.

[15] Yarnykh VL. Actual flip-angle imaging in the pulsed steady state: a method for rapid three-dimensional mapping of the transmitted radiofrequency field *Magn Reson Med.* 2007;57:192–200.

[16] Pohmann R, Scheffler K. A theoretical and experimental comparison of different techniques for B1 mapping at very high fields *NMR Biomed.* 2013;26:265–275.

[17] Matsuda Tsuyoshi, Uwano Ikuko, Iwadate Yuji, Yoshioka Kunihiro, Sasaki Makoto. Spatial and temporal variations of flip-angle distributions in the human brain using an eight-channel parallel transmission system at 7T: comparison of three radiofrequency excitation methods *Radiological Physics and Technology.* 2021;14:161–166.

[18] Wu Xiaoping, Deelchand Dinesh Kumar, Yarnykh Vasily L, Ugurbil Kmil, Moortele Pierre-Franois. Actual flip angle imaging: From 3D to 2D in *Proceedings of the 17th Annual Meeting of ISMRM*:372 2009.

[19] Hurley SA, Yarnykh VL, Johnson KM, Field AS, Alexander AL, Samsonov A. Simultaneous variable flip angle–actual flip angle imaging method for improved accuracy and precision of three-dimensional T1 and B1 measurements *Magn Reson Med.* 2012;68:54–64.

[20] Maggioni MB, Krämer M, Reichenbach JR. Optimized gradient spoiling of UTE VFA-AFI sequences for robust T1 estimation with B1-field correction *Magn. Reson. Imaging.* 2021.

[21] Busse RF, Riederer SJ. Steady-state preparation for spoiled gradient echo imaging *Magn Reson Med.* 2001;45:653–661.

[22] Voigt T, Nehrke K, Doessel O, Katscher U. T1 corrected B1 mapping using multi-TR gradient echo sequences *Magn Reson Med.* 2010;64:725–733.

[23] Balezeau FA, Eliat PA, Cayamo AB, Saint-Jalmes H. Mapping of low flip angles in magnetic resonance

[24] Liberman G, Louzoun Y, Ben Bashat D. T1 mapping using variable flip angle SPGR data with flip angle correction *J. Magn. Reson. Imaging.* 2014;40:171–180.

[25] Boudreau M, Tardif CL, Stikov N, Sled JG, Lee W, Pike GB. B1 mapping for bias-correction in quantitative T1 imaging of the brain at 3T using standard pulse sequences *J. Magn. Reson. Imaging.* 2017;46:1673–1682.

[26] Ma YJ, Lu X, Carl M, et al. Accurate T1 mapping of short T2 tissues using a three-dimensional ultrashort echo time cones actual flip angle imaging-variable repetition time (3D UTE-Cones AFI-VTR) method *Magn Reson Med.* 2018;80:598–608.

[27] Wei Z, Jang H, Bydder GM, Yang W, Ma YJ. Fast T1 measurement of cortical bone using 3D UTE actual flip angle imaging and single-TR acquisition (3D UTE-AFI-STR) *Magn Reson Med.* 2021;85:3290–3298.

[28] Malik Shaihan J, Kenny Gavin D, Hajnal Joseph V. Slice profile correction for transmit sensitivity mapping using actual flip angle imaging *Magnetic resonance in medicine.* 2011;65:1393–1399.

[29] Bernstein MA, King KF, Zhou XJ. *Handbook of MRI pulse sequences.* Elsevier 2004.

[30] Hennig J. Echoes—how to generate, recognize, use or avoid them in MR-imaging sequences. Part I: Fundamental and not so fundamental properties of spin echoes *Concepts Magn Reson.* 1991;3:125–143.

[31] Hennig J. Echoes—how to generate, recognize, use or avoid them in MR-imaging sequences. Part II: Echoes in imaging sequences *Concepts Magn Reson.* 1991;3:179–192.

[32] Weigel M. Extended phase graphs: dephasing, RF pulses, and echoes-pure and simple *J. Magn.* 2015;41:266–295.

[33] Tannús A, Garwood M. Adiabatic pulses *NMR Biomed.* 1997;10:423–434.

[34] Sass M, Ziessow D. Error analysis for optimized inversion recovery spin-lattice relaxation measurements *J. Magn. Reson.* 1977;25:263–276.

[35] Kowalewski J, Levy GC, Johnson LRF, Palmer L. A three-parameter non-linear procedure for fitting inversion-recovery measurements of spin-lattice relaxation times *J. Magn. Reson.* 1977;26:533–536.

[36] Zampini MA, Sijbers J, Verhoye M, Garipov R. EPIFANI for ultrafast B1-corrected T1 and PD mapping in *Proc., ESMRMB, 38th Annual Scientific Meeting*;34:59–60 2021.

[37] Yarnykh VL. Optimal radiofrequency and gradient spoiling for improved accuracy of T1 and B1 measurements using fast steady-state techniques *Magn Reson Med.* 2010;63:1610–1626.

[38] Sattin W. A rapid high signal to noise ratio RF calibration scheme in *Proc., SMRM, 7th Annual Meeting*:1016 1988.

[39] Ogg Robert J, Kingsley RB, Taylor June S. WET, a T1-and B1-insensitive water-suppression method for in vivo localized 1H NMR spectroscopy *Journal of Magnetic Resonance, Series B.* 1994;104:1–10.

[40] Yamashiro A, Kobayashi M, Saito T. Cerebrospinal fluid T1 value phantom reproduction at scan room temperature *J. Appl. Clin. Med. Phys..* 2019;20:166–175.

[41] Kent James L, Dragonu Iulius, Valkovič Ladislav, Hess Aaron T. Rapid 3D absolute B1+ mapping using a sandwiched train presaturated TurboFLASH sequence at 7 T for the brain and heart *Magnetic Resonance in Medicine.* 2023;89:964–976.

[42] Jordanova Kalina V, Nishimura Dwight G, Kerr Adam B. B1 estimation using adiabatic refocusing: BEAR *Magnetic Resonance in Medicine.* 2014;72:1302–1310.

[43] Chang Yulin V. Rapid B1 mapping using orthogonal, equal-amplitude radio-frequency pulses *Magnetic Resonance in Medicine.* 2012;67:718–723.

[44] Jiru Fast, Klose U. Fast 3D radiofrequency field mapping using echo-planar imaging *Magnetic Resonance in Medicine: An Official Journal of the International Society for Magnetic Resonance in Medicine.* 2006;56:1375–1379.

[45] Chung Sohae, Kim Daniel, Breton Elodie, Axel Leon. Rapid B1+ mapping using a preconditioning RF pulse with TurboFLASH readout *Magnetic resonance in medicine.* 2010;64:439–446.

[46] Sacolick Laura I, Wiesinger Florian, Hancu Ileana, Vogel Mika W. B1 mapping by Bloch-Siegert shift *Magnetic resonance in medicine.* 2010;63:1315–1322.

[47] Brenner Daniel, Tse Desmond HY, Pracht Eberhard D, Feiweier Thorsten, Stirnberg Rüdiger, Stöcker Tony. 3DREAM—a three-dimensional variant of the DREAM sequence in *Proceedings of the 22nd scientific meeting, International Society for Magnetic Resonance in Medicine, Milan*;1455 2014.

[48] Nehrke Kay. On the steady-state properties of actual flip angle imaging (AFI) *Magnetic Resonance in Medicine: An Official Journal of the International Society for Magnetic Resonance in Medicine.* 2009;61:84–92.

[49] Ehses Philipp, Brenner Daniel, Stirnberg Rüdiger, Pracht Eberhard D, Stöcker Tony. Whole-brain B1-mapping using three-dimensional DREAM *Magnetic Resonance in Medicine.* 2019;82:924–934.

[50] Bouhrara Mustapha, Spencer Richard G. Steady-state double-angle method for rapid B1 mapping *Magnetic resonance in medicine.* 2019;82:189–201.

[51] Wilman Alan H, Riederer Stephen J. Performance of an elliptical centric view order for signal enhancement and motion artifact suppression in breath-hold three-dimensional gradient echo imaging *Magnetic resonance in medicine.* 1997;38:793–802.

[52] Wang Haonan, Bangerter Neal K, Park Daniel J, et al. Comparison of centric and reverse-centric trajectories for highly accelerated three-dimensional saturation recovery cardiac perfusion imaging *Magnetic resonance in medicine.* 2015;74:1070–1076.

[53] Chuang Kai-Hsiang, Koretsky Alan. Improved neuronal tract tracing using manganese enhanced magnetic resonance imaging with fast T1 mapping *Magnetic Resonance in Medicine: An Official Journal of the International Society for Magnetic Resonance in Medicine.* 2006;55:604–611.

[54] Cunningham Charles H, Pauly John M, Nayak Krishna S. Saturated double-angle method for rapid B1+ mapping *Magnetic Resonance in Medicine: An Official Journal of the International Society for Magnetic Resonance in Medicine.* 2006;55:1326–1333.

[55] Abbasi-Rad Shahrokh, Saligheh Rad Hamidreza. Quantification of human cortical bone bound and free water in vivo with ultrashort echo time MR imaging: a model-based approach *Radiology.* 2017;283:862–872.

[56] Zur Y, Wood ML, Neuringer LJ. Spoiling of transverse magnetization in steady-state sequences *Magn Reson Med.* 1991;21:251–263.

[57] Epstein FH, Mugler III JP, Brookeman JR. Spoiling of transverse magnetization in gradient-echo (GRE) imaging during the approach to steady state *Magn Reson Med.* 1996;35:237–245.

[58] Sekihara K. Steady-state magnetizations in rapid NMR imaging using small flip angles and short repetition intervals *IEEE Trans Med Imaging.* 1987;6:157–164.

[59] Preibisch C, Deichmann R. Influence of RF spoiling on the stability and accuracy of T1 mapping based on spoiled FLASH with varying flip angles *Magn Reson Med.* 2009;61:125–135.

[60] Baudrexel S, Nöth U, Schüre J-R, Deichmann R. T1 mapping with the variable flip angle technique: a simple correction for insufficient spoiling of transverse magnetization *Magn Reson Med.* 2018;79:3082–3092.

[61] Hargreaves BA, Miller KL. Using extended phase graphs: review and examples in *Proceedings of the 21st Annual Meeting of ISMRM*:3718 2013.

Supplementary materials

S1 Steady-state approach with dummy pulses in SPGR

A perfectly spoiled SPGR signal follows the well-known expression

$$S_{SPGR} = M_0 \sin\alpha \cdot \frac{1-E_1}{1-E_1\cos\alpha} \exp(-\mathrm{TE}/\mathrm{T}_2^*) \quad . \tag{S.1}$$

Starting from Bloch equations and assuming perfect spoiling, the steady-state magnetization for an SPGR sequence can be retrieved. The transverse magnetization is zero just before each new pulse, which then converts longitudinal magnetization into transverse magnetization. If M_z is M_{zA}, then after the RF pulse $M_{zB} = M_{zA}\cos\alpha$ and, after relaxation, magnetization would become $M_{zC} = M_{zB}e^{-TR/T_1} + M_0(1-e^{-TR/T1}) = M_{zA}\cos\alpha E_1 + M_0(1-E_1)$ where $E_1 = e^{-TR/T_1}$. The steady state condition is reached for longitudinal magnetization when $M_{zA} = M_{zC}$, which yields

$$\frac{M_{zA}}{M_0} = \frac{1-E_1}{1-\cos\alpha E_1} = f_{z,ss} \tag{S.2}$$

so that the approach to steady state (transient state) at the j-th pulse of an SPGR sequence can be expressed as

$$S_j = M_0 \sin\alpha e^{-TE/T_2^*}[f_{z,ss} + (\cos\alpha E_1)^{j-1}(1-f_{z,ss})] \quad . \tag{S.3}$$

In Figure **??** we report a level plot of the number of pulses required for a relative error $\epsilon < 5\%$ for a SPGR sequence without preparation, where the signal was simulated via Equation S.3. Counter-intuitively, the smaller the flip angle is, the higher the amount of dummy pulses/discarded acquisitions is required to approach reliably the SS in SPGR-based sequences, which may require hundreds of dummy pulses for a 5-10% accuracy in terms of absolute distance between the signal intensity and the SS value.

For AFI (shown in Figure **??**), flip angle, $\mathrm{TR}_1/\mathrm{T}_1$, and the error threshold ϵ have significant effect on the number of dummies required. The black arrow shows the shift direction of the level lines towards the left of the plot. With respect to an AFI acquisition with analogous parameters (and $n > 1$), the number of dummy pulses for reaching signal accuracy is higher, and can reach hundreds for low flip angle amplitudes and long T_1 values.

S2 Derivation of Equation 6

Matching the magnetization after an arbitrary β plse and a free relaxation period T_{rec} to the SS magnetization of the AFI sequence we get Equation 5:

$$T_{rec} = \mathrm{T}_1 \log\left(\frac{1-\cos\beta}{1-A_1}\right) \overset{\beta=\pi/2}{=} -\mathrm{T}_1\log(1-A_1) \tag{S.4}$$

which, for $\mathrm{T}_1 \to +\infty$, brings to an indeterminate form of the type $\infty\cdot 0$. With a first order approximation via Taylor series, this becomes

$$T_{rec} \approx \mathrm{T}_1 A_1 = \mathrm{T}_1 \frac{1-E_2+(1-E_1)E_2\cos\alpha}{1-E_1E_2\cos^2\alpha} \tag{S.5}$$

and expanding $E_{1,2}$ as $1 - \mathrm{TR}_{1,2}/\mathrm{T}_1$, this leads to

$$T_{rec} \approx \frac{\mathrm{TR}_2 + \mathrm{TR}_1 \cos\alpha}{1 - \cos^2\alpha} = \mathrm{TR}_1 \frac{n + \cos\alpha}{1 - \cos^2\alpha} \quad \blacksquare \tag{S.6}$$

Also, the partial derivative of T_{rec} in $\partial \mathrm{T}_1$ from Equation 5 is

$$\frac{\partial T_{rec}}{\partial \mathrm{T}_1} = \frac{N_1 A_1 + N_2}{T_1^2 D_1 (1 - A_1)} - \log(1 - A_1) \tag{S.7}$$

with $N_1 = \cos^2\alpha E_1 E_2 * \mathrm{TR}_1(n+1)$, $N_2 = \mathrm{TR}_1(-\cos\alpha E_1 E_2 + n\cos\alpha(1-E_1)E_2 - nE_2)$, and $D_1 = (1 - \cos^2\alpha E1E2)$.

The plot for $\alpha = 60°$, $\mathrm{TR}_1 = 50$ ms, and $n = 5$ (matching the values for Figure **??**) is reported in Figure **??**. This shows the approach to a T_1 independent T_{rec} for increasing T_1 values. The minimum T_1 value that leads to a partial derivative smaller than $\epsilon = 10\%$ (arbitrarily chosen) for $\mathrm{TR}_1 \in [0.001, 0.1]$, $\alpha \in [30, 80]°$, and $n = 4, 5, 6$ is reported in Figure **??**. For increasing flip angle and ϵ, and smaller n factors, the minimum T_1 decreases, while longer TR_1 values come with longer minimum T_1s.

S3 Signal spoiling

The pivotal Equations 1 and S.1 are only valid for complete spoiling of transverse magnetization before each excitation pulse, which can be reached by gradient and RF spoiling. RF spoiling, in particular, requires a model for cycling the RF phase to avoid coherence build-up that spoils the transverse magnetization, and in a popular method[56,57,58], the phase of the k-th RF pulse is cycled as

$$\phi_k = \phi_{k-1} + k\phi_0 \quad k = 1, 2, 3, ... \tag{S.8}$$

with ϕ_0 being the phase-cycling characteristic. Nevertheless, standard RF spoiling is generally insufficient both in VFA and in AFI, which may yield systematic errors in parameter quantification, so several methods for efficient signal spoiling have been proposed, such as corrections to T_1 maps[59], the use of effective excitation angles[60] or the introduction of very strong spoiling gradients[37]. We selected the last approach, and investigated the influence of RF pulse phase characteristic ϕ_0 on the behavior of the signal after the application of the preparation pulse.

The spoiling features for a prepared AFI sequence were obtained via Extended Phase Graph simulations. The signal from AFI sequence with the implementation of the preparation module was simulated to check spoiling characteristics including the effects of $\mathrm{T}_1 \in [0.5; 4.5]$ s, $\mathrm{T}_2 \in [0.01; 1.0]$ s, gradient spoiling = 327 and 1415 mT·ms/m (high spoiling regime) for TR_1 and TR_2, respectively, TE = 5 ms and diffusion coefficient $D \in [0; 2] \cdot 10^{-3}$ mm^2/s following the approach of Hargreaves[61] and Weigel[32]. $\mathrm{TR}_1 = 20$ ms, $n = \mathrm{TR}_2/\mathrm{TR}_1 = 5$ and $\alpha = 60°$ were chosen from literature values[19,15] for simulations and then used during scanning.

S3.1 Results

The RF pulse spoiling phase characteristic for both AFI_1 and AFI_2 signals for a range of physiological values with the preparation module shows the same features as the signals in a not-prepared AFI sequence. As shown in Figure **??**, the periodicity of the original AFI signals is maintained (the symmetry

around 90° and 180° period). The minimum distance between the median values and the perfectly spoiled SS value for AFI_1 and AFI_2 are found in the different locations along the RF increment range. Nevertheless, the common minimum distance to the steady-state values (represented by the zero horizontal line) for median values is observed in the region of ϕ_0 = 20-25° for all n values investigated. This RF phase increment for the AFI sequence also corresponds to a local minimum of the sum of the absolute distances from the steady state for the whole range of T_1, T_2 and D considered. For both simulations and experiments with AFI sequences, we used an RF pulse with spoiling phase characteristic ϕ_0 of 25°.

S3.2 Discussion

An RF phase increment for a wide range of physiological parameters (T_1, T_2 and D) in the high gradient spoiling regime was reported. The $\phi_0 = 25°$ appears to minimize the variability of AFI_1 around the steady state and matches the region of small AFI_2 variability as well. This RF increment indeed minimizes both the overall median difference and range to the ideal steady-state value for a range of n values. Nevertheless, this is specific to the sequence parameters we used (TR_1 = 20 ms, $\alpha = 60°$, high spoiling regime) and users are advised to run simulations with their own system and sequence specifics.

Tables

Table 1: Parameters used for AFI simulations reported in this study. The rows of parameters have been used in the referenced Figures of the first column.

Simulations	TE/TR$_1$ [ms]	α [°]	ϕ_0 [°]	κ	n	T$_1$ [s]	T$_2$ [s]	D [$\cdot 10^{-3}$ mm^2/s]	T_{rec} [ms]
Fig. 1	3/20	0 - 90	-	1	5	0.4 - 4	-	-	-
Fig. 2a	3/50	60	-	1	5	0 - 5	-	-	366
Fig. 3, 4	3/20	60, 30	25	1	5	2.52	0.01	1	147, 469
Fig. 5	3/20	40	25	1	5	1.5	0.01 - 0.2	1	279

Table 2: Parameters used for the AFI experiments reported in this study. The rows of parameters have been used in the referenced Figures of the first column.

Experiments	TE/TR$_1$ [ms]	α [°]	ϕ_0 [°]	n	T$_1$ [s]	B$_0$ [T]	T_{rec} [ms]
Fig. 3, 4	3/20	60	25	5	2.52	4.7	147
Fig. 6a, 6b, 6c	3/200	60	25	4	2.52	7	1200
Fig. 6d	3/200	60	25	4	1.11 - 2.59	7	1200
Fig. 7	3/100	60	37	5		7	733
Fig. 8	23/300	60	37	5		7	3666

1 Figures

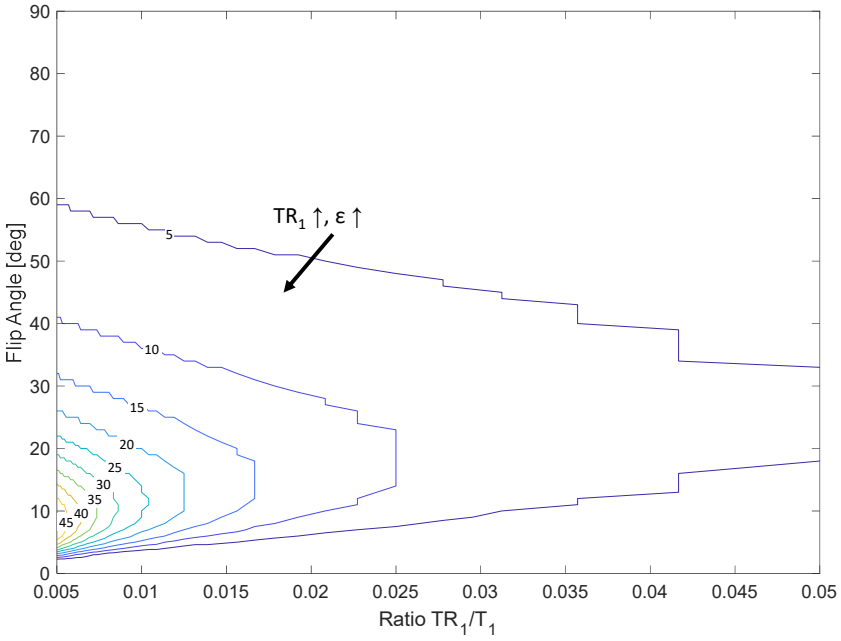

Figure 1: Level plot of the number of pulses required for a relative error $\epsilon < 5\%$ for an AFI sequence without preparation. Flip angle, the $\mathrm{TR}_1/\mathrm{T}_1$, n and the error threshold ϵ have an effect on the minimum number of dummies required, shifting the level lines towards the left of the plot, as indicated by the black arrow.

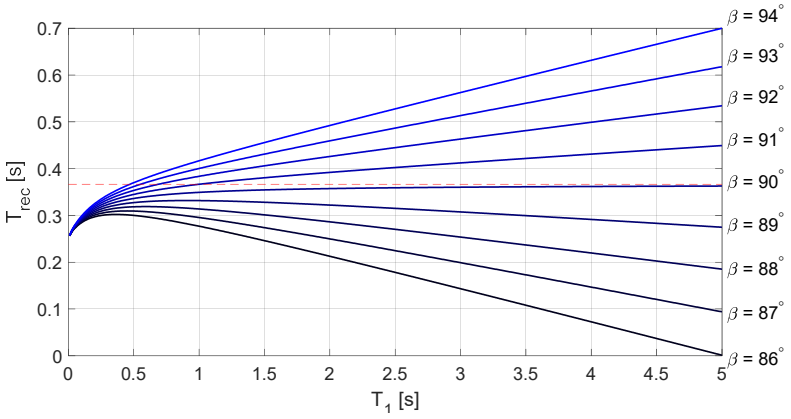

(a)

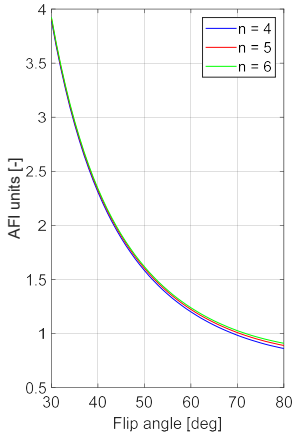

(b)

Figure 2: a: Dependency of the recovery time T_{rec} and flip angle for AFI_1 (continuous line) signal following the adiabatic preparation pulse over T_1, for different β values ranging from 86° to 94°, with α = 60°, TR_1 = 50 ms, $n = 5$. Asymptotic value for $T_1 \to \infty$ is shown in red (dashed line at T_{rec} = 366.6 ms, compared to a single AFI dummy cycle of $TR_1(n+1)$ = 300 ms). b: T_{rec} time normalized by the duration of an AFI sequence for increasing flip angle. An AFI unit corresponds to the duration of a full AFI acquisition, namely $TR_1(n+1)$. The recovery time following the described preparation module is shorter than 4 full AFI units.

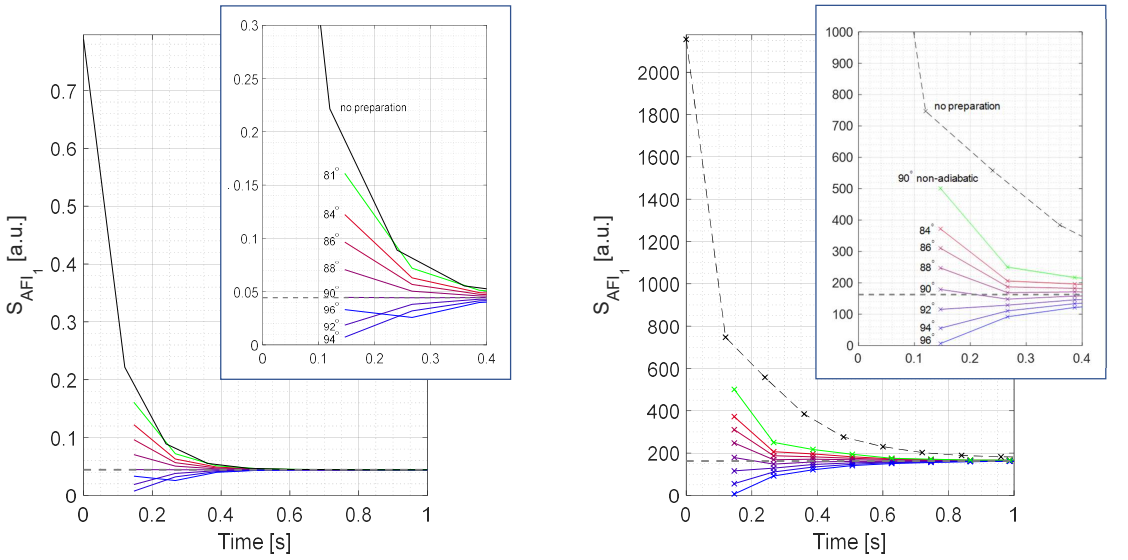

(a)

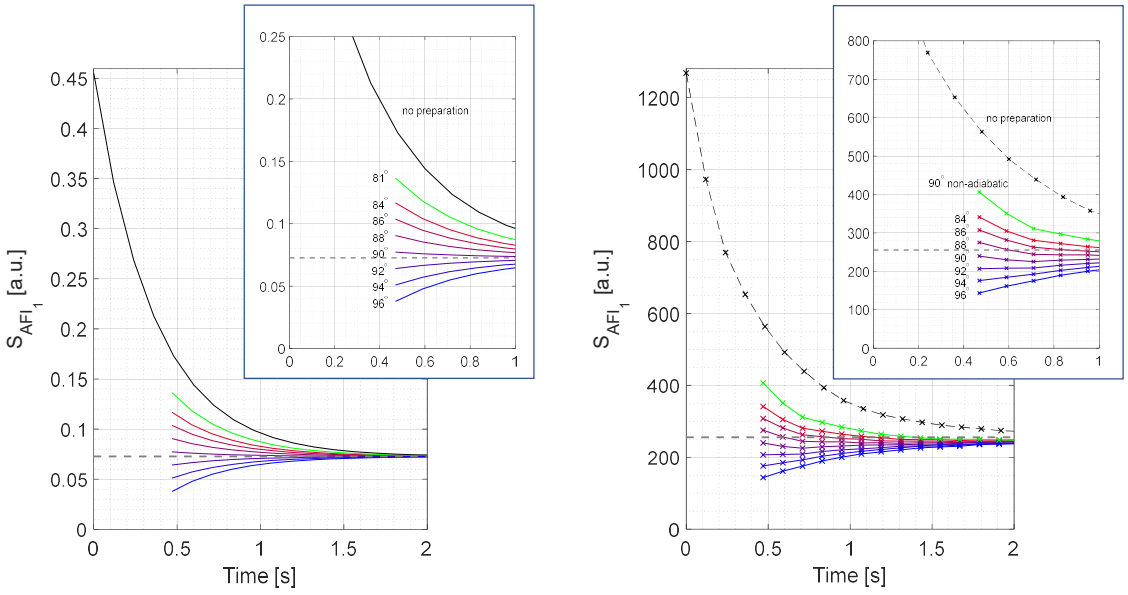

(b)

Figure 3: EPG simulations (left) and experimental results (right) on the variation of β amplitude for AFI with $\alpha = 60°$ (a) and 30° (b). The upper right boxes show a magnification of the signal for the first RF pulses. Graphs on the right also show a comparison between the signal behavior when prepared via adiabatic RF pulses (β ranging from 84° to 96°) and a non-adiabatic RF pulse ($\beta = 90°$) – the amplitude of the non-adiabatic pulses was scaled by the κ factor computed via AFI for simulations. Median SS value is reported as gray dashed lines. The values of the parameters used for both simulations and experiments are found in Table 1 and 2, respectively.

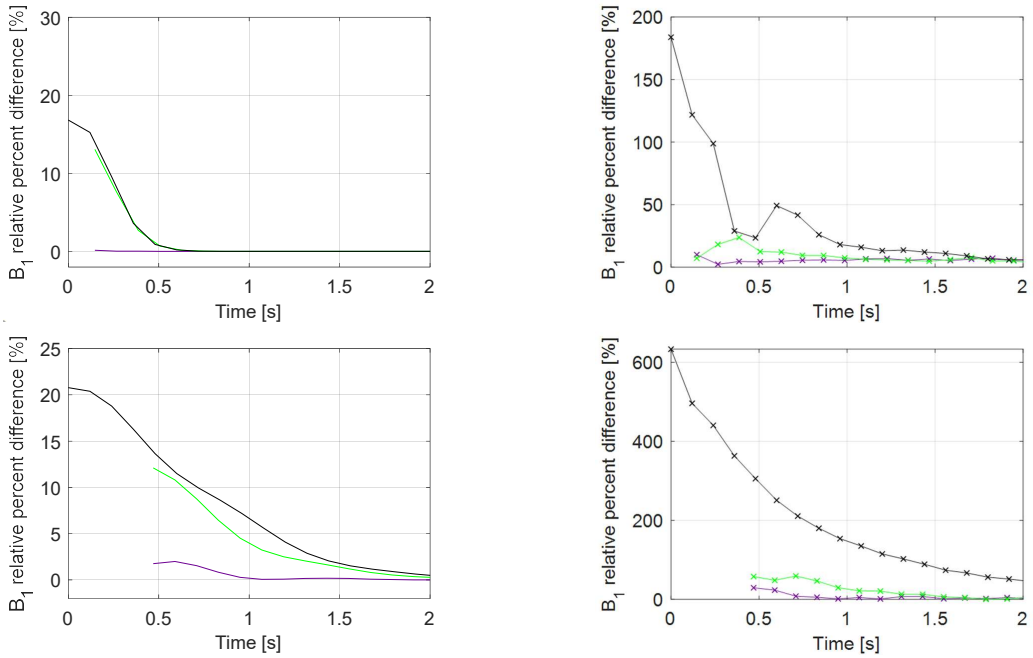

Figure 4: B_1 relative percent difference computed for both simulations (left column) and experimental data (right column), for $\alpha = 60°$ (top) and 30° (bottom). Black line refers to data acquired without any preparation module, green refers to data acquired with a 90° non-adiabatic preparation pulse, and purple refers to data acquired with a preparation pulse featuring an adiabatic pulse with $\beta = 90°$.

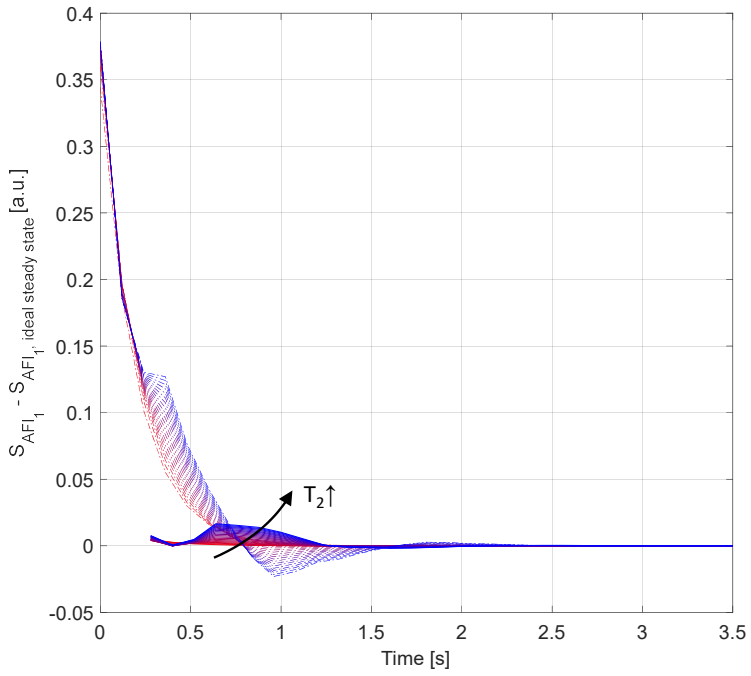

Figure 5: Simulated approach to steady state without (dashed line) and with (continuous line) preparation pulse for AFI_1 for $T_1 = 1.5$ s, $\alpha = 40°$, $D = 1 \cdot 10^{-3}$ mm^2/s, T_2 ranging from 0.01 to 0.2 s (increasing T_2 values are represented by a shift from red to blue color and are indicated by the black arrow).

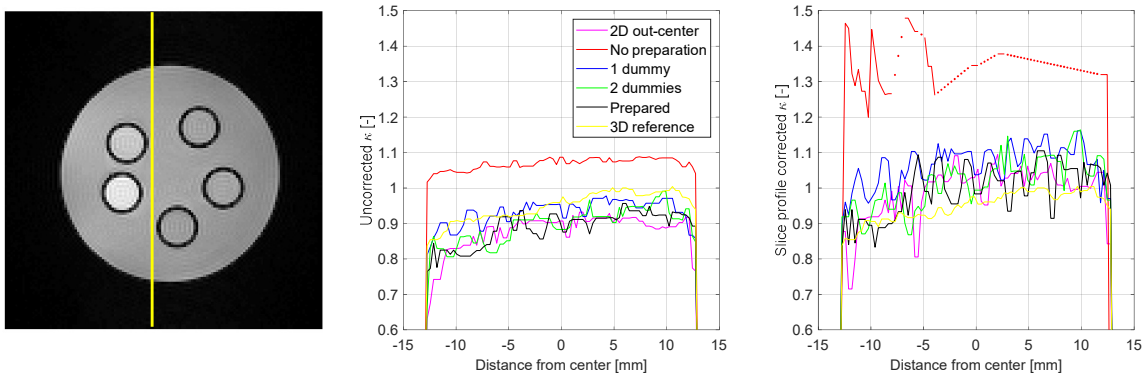

(a)

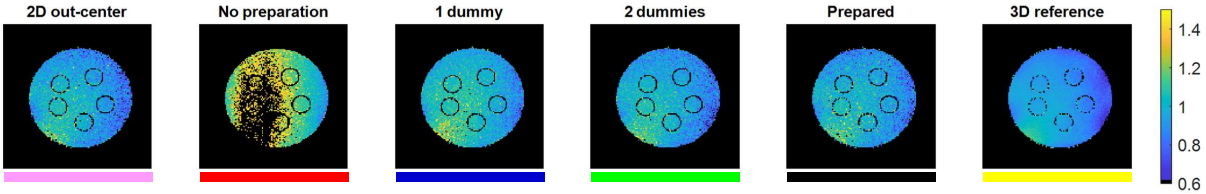

(b)

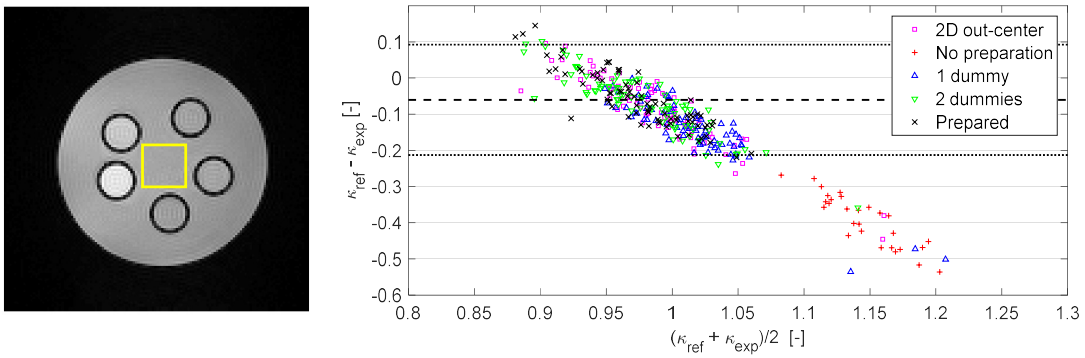

(c)

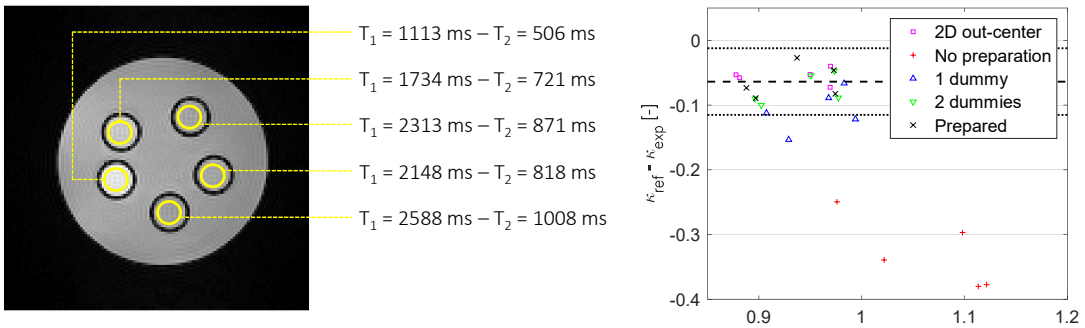

(d)

Figure 6: Phosphate-buffered saline solution phantom. a: Example for κ (normalized B_1) profile along the yellow line for values uncorrected and corrected for the slice profile effects. b: Slice profile corrected normalized B_1 maps for acquisitions performed with an out-center scheme, with no preparation, with a single dummy scan, with two dummy scans, with the proposed preparation pulse, and from a 3D reference acquisition. Pixels belonging to the background and whose values that can not be mapped based on the slice correction are black. Colors found under the image refer to the respective colors in the other plots. c, d: Bland-Altman plots for the normalized B_1 values found (c) in the central area of the sample reported as a yellow rectangle and (d) in the 5 Gadolinium solutions reported as a yellow rectangle. Values are compared against the 3D reference. Mean (dashed line) and values at 2 standard deviations from the mean (dotted lines) refer to the B_1 values for a prepared acquisition.

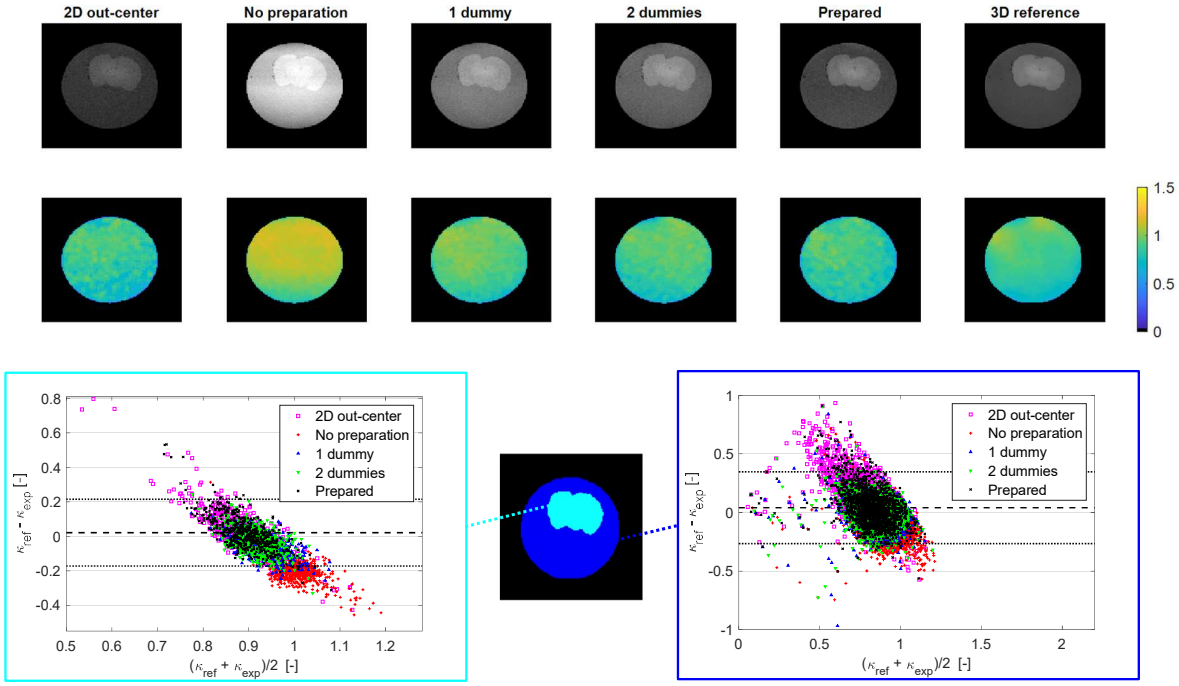

Figure 7: Examples of AFI_1 images (first row) and corresponding κ maps of data acquired on an ex vivo mouse brain with a conventional 2D out-center k-space trajectory, and for center-out trajectories with no preparation, one and two dummy pulses, with the proposed preparation module, and with a 3D acquisition. Bland-Altman plots referring to both the mouse brain (bottom left) and the agar (bottom right) are reported.

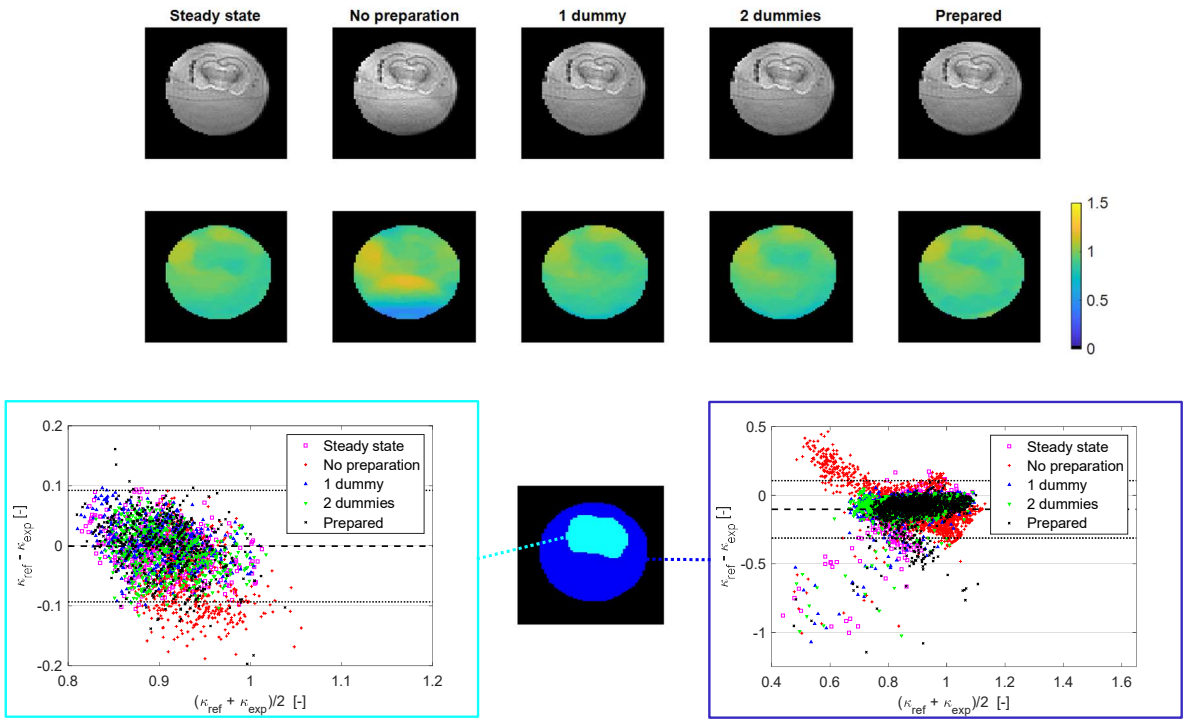

Figure 8: Examples of AFI_1 images (first row) and corresponding κ maps of data acquired with EPI readout (EPIFANI) on an ex vivo mouse brain. Acquisitions at steady-state, without preparation, with one and two dummy pulses, and with the proposed preparation module are reported. With respect to AFI images, EPIFANI is able to show that the mouse brain is enclosed in a capsule - note the horizontal line at the center of the sample. A 3x3 median filter was applied on the κ maps (second row) to better represent the slowly varying B_1 field. Bland-Altman plots referring to both the mouse brain (bottom left) and the agar (bottom right) are reported.

Figures - Supplementary Materials

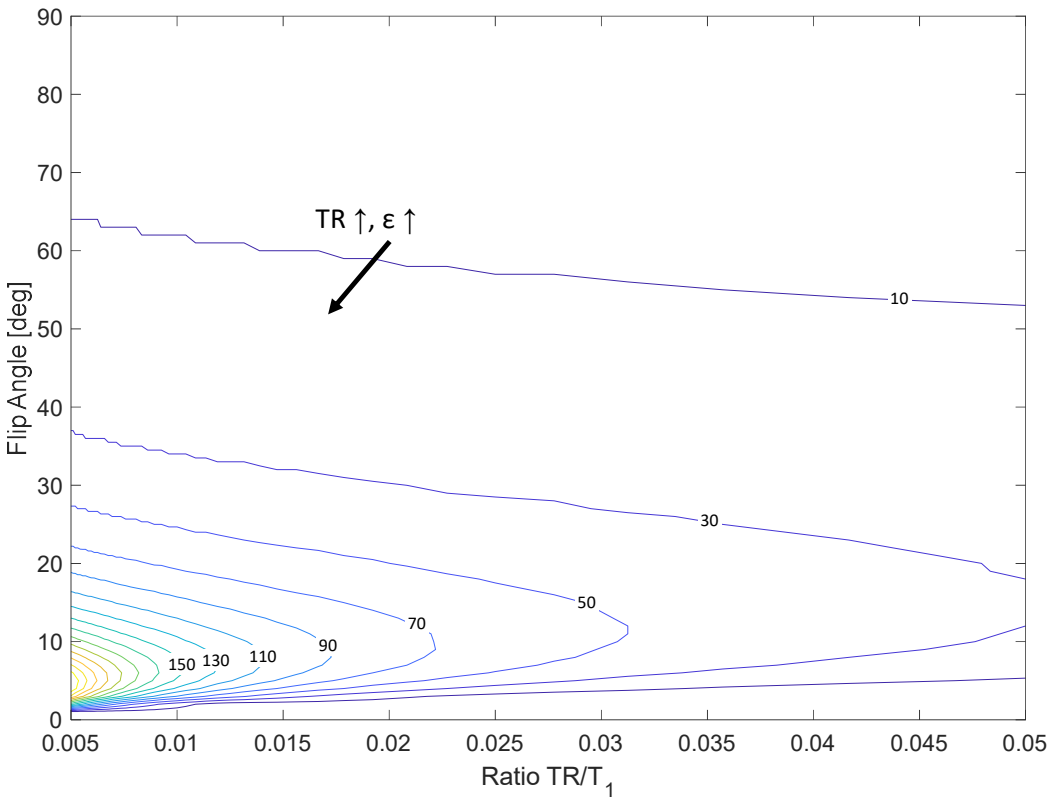

Figure 9: Level plot of the minimum number of pulses required for a relative error $\epsilon < 5\%$ for an SPGR sequence without preparation.

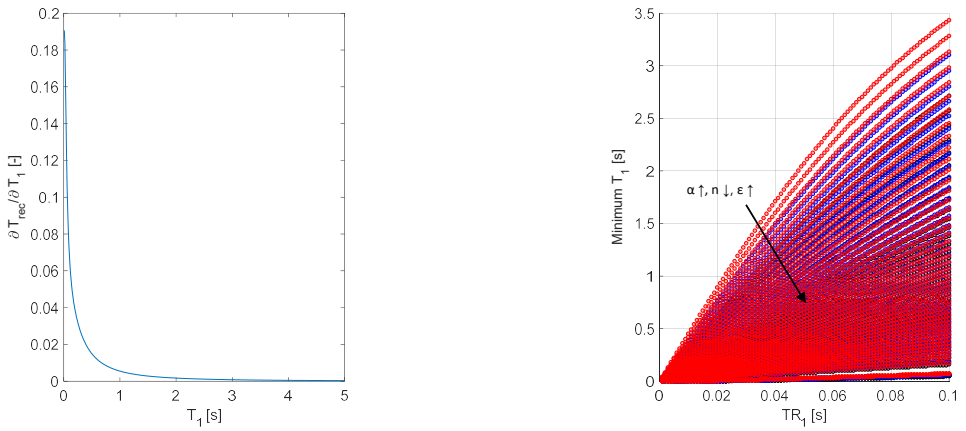

(a) (b)

Figure 10: a: Partial derivative $\partial T_{rec}/\partial$ T$_1$ for $\alpha = 60°$, TR$_1$ = 50 ms, $n = 5$, $z = 1$. b: Minimum T$_1$ value for $\partial T_{rec}/\partial$T$_1 < 0.05$ for TR$_1 \in$ [0.02,0.1], $\alpha \in [30, 80]°$, $n = 4$ (black), 5 (blue), 6 (red).

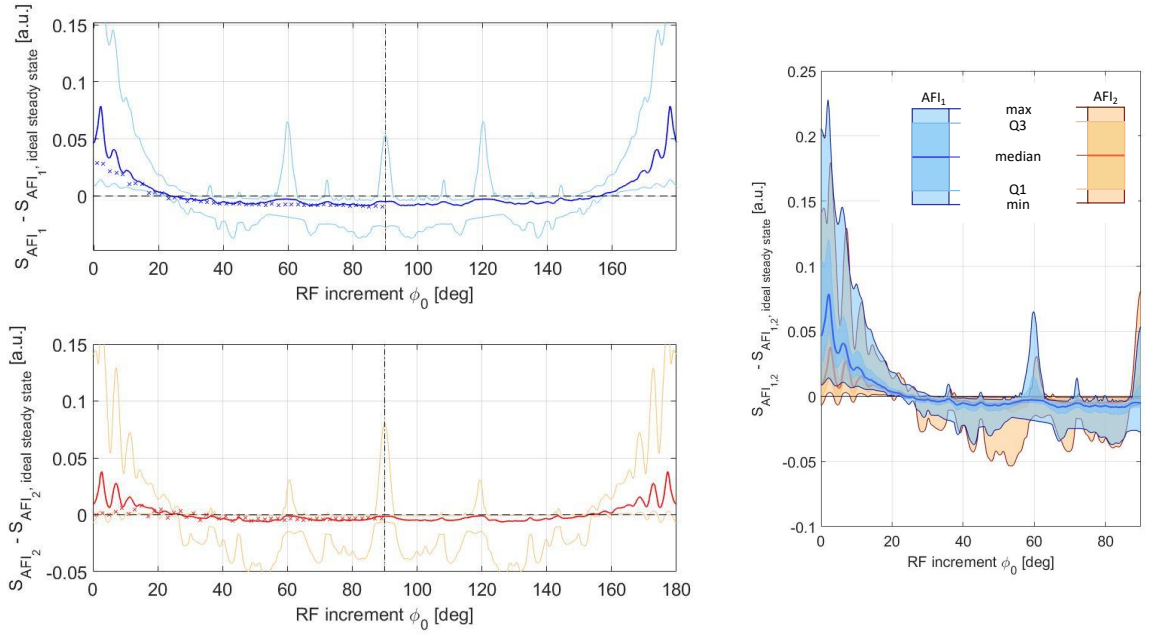

Figure 11: Left: Using a RF pulse phase characteristic ϕ_0 can result in a bias of AFI signals with respect to SS signal, and this bias also depends on the sample properties. Upper and lower lighter lines represent the maximum and the minimum of the distributions for $TR_1 = 20$ ms, $T_1 \in [0.5; 4.5]$ s, $T_2 \in [0.01; 1.0]$ s, gradient spoiling = 327/1415 mT·ms/m (for TR_1 and TR_2, respectively, corresponding to a high spoiling regime), $D \in [0; 2] \cdot 10^{-3}$ mm^2/s, $n = 5$ and $\alpha = 60°$. Crosses represent experimental data for a water phantom ($T_1 = 2.09$ s, $T_2 = 1.08$ s). Right: Median (blue), interquartile range (dark shaded area) and range (light shaded area) values also show a variation over the common sequence and tissue parameters with respect to the SS value (black dashed line). Minimum values for AFI_1 and AFI_2 can be found for different RF increment values, but a range characterized by small ranges and minimum bias is common for both signals around 25°.